8. Adsorption of carbon monoxide on Au(110)-(1×2)

In the preceding chapters, we discussed the spontaneous oxygen adsorption, which occurs only at low temperatures, and the preparation of a reactiv, atomically chemisorbed oxygen species, which requires external activation of the O_2/Au system, e.g. by electron bombardment. Before we embark on the kinetics of the CO oxidation reaction in Chapter 11, we have to consider the other reactand, CO. In the present chapter, we report results of a combined TDS, UPS, Δφ, LEED, and NEXAFS study concerning CO adsorption on Au(110)-(1x2) under UHV conditions at temperatures down to 28 K. Furthermore, we studied the coadsorption of CO and krypton to get information about the possible adsorption sites of CO.

As already mentioned, the interest in catalysis by supported gold nanoparticles has rapidly grown during the past 15 years [Ha87, Ha97], both scientifically and industrially. Most activity has focussed on the CO oxidation reaction [Bo99, Bo00, Gr02], which is catalysed by these materials even below room temperature and which is of high importance e.g. for automotive pollution abatement [Me02] and for producing CO-free hydrogen gas suitable for fuel cells. The mechanism of the CO oxidation and the nature of the active centres on these gold catalysts are still controversial. However, recent studies provided evidence that CO adsorbs on the gold particles [De98, De99], in contrast to O_2, which appears to adsorb preferentially at sites on the junction of Au cluster and support [Bo00]. These findings make the CO-gold interaction an interesting topic also for a model study on a gold single-crystal surface.

Apart from several reports concerning supported gold particles and polycrystalline films, CO adsorption has previously been investigated mainly on polycrystalline gold and on the (100)-, (110)-, and (332)-surfaces of gold. Norton et al. [No78] measured UV photoemission spectra of CO on a polycrystalline gold foil and found evidence for a chemisorptive CO-metal bond. CO adsorption on Au(100) at 81.5 K was studied by McElhiney and Pritchard [Mc76a] using LEED, EELS, and Δφ measurements. As in all subsequent reports, no CO phases with long-range order were observed. The authors determined an initial isosteric heat of adsorption, Q_{st}, of 58 kJ/mol, using Δφ as a coverage monitor. This value agreed well with earlier reports on CO adsorption on polycrystalline gold films [Lo72]. More recently, Dückers and Bonzel [Dü89] studied CO adsorption on Au(110) with photoemission spectroscopy at 117 K, a temperature which allows, according to our measurements, only CO coverages < 0.33 ML in UHV. Sandell et al. [Sa94] performed similar studies at l-N_2 temperature, which limits the CO coverage to < 0.5 ML. Extensive LEED, TDS, Δφ, and RAIRS studies of CO adsorption on Au(332) at 92 K and 105 K were performed by Ruggiero and Hollins [Ru96, Ru97]. For this surface, an initial isosteric heat of adsorption of 55 kJ/mol was determined.

UHV studies focussing on the low-temperature and, thus, high-coverage range below 77 K have not been carried out so far. At ambient temperatures, high CO coverages can still be obtained by raising the CO gas pressure. Making use of this possibility, a com-

bined RAIRS and STM investigation of CO on Au(110) at 300 K and elevated CO pressures up to 500 torr was recently reported [Ju02]. The authors found weakly chemisorbed CO with a C-O stretching frequency of ν_{CO} = 2110 cm^{-1} at pressures above 10^{-2} torr and another, probably physisorbed species with ν_{CO} = 2141 cm^{-1} at ≥ 100 torr. Unfortunately, high gas pressures lead to methodical limitations and problems with sample contamination due to gas impurities.

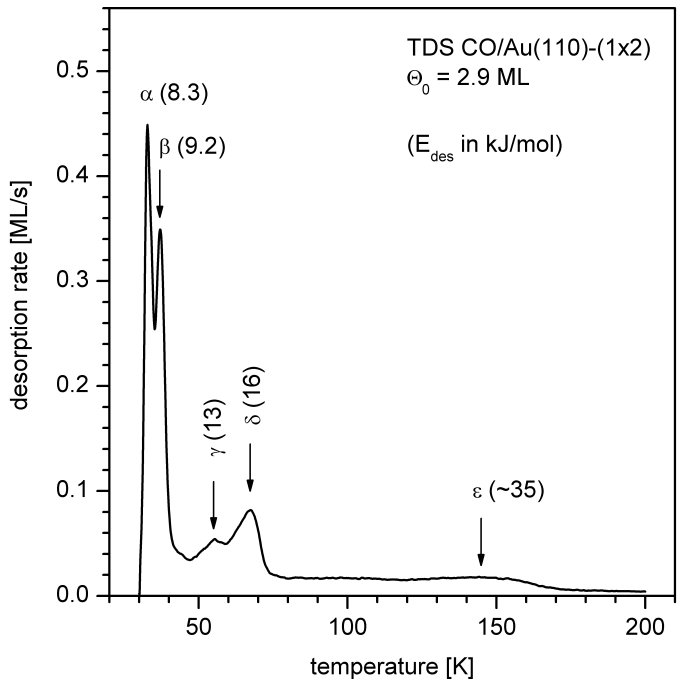

Fig. 8.1: TDS CO/Au(110)-(1×2) for an initial coverage of 2.9 ML (9 L). Heating rate 2.35 K/s, CO^+ detection (m/z = 28). Dosing pressure[1] 2×10^{-8} mbar. The desorption activation energies (in kJ/mol) for the first-layer peaks γ-ε were calculated after Redhead [Re62], those for α and β were obtained by leading-edge analysis [Ha84]. The first-order frequency factors for γ-ε were approximated by k_BT_{max}/h with the respective desorption temperatures T_{max} (marked by arrows). Experimental details of the TD measurements can be found in Section 4.1.2.

8.1. Thermal desorption spectroscopy (TDS)

CO DESORPTION FROM WELL-ORDERED AU(110)-(1×2) – Fig. 8.1 shows a CO TD spectrum corresponding to an initial coverage of 2.9 ML, which is sufficient to populate all five desorption states. The broad ε peak between 75 K and 180 K with a maximum at T_{max} = 145 K and the peaks δ (67 K) and γ (55 K) are attributed to the

[1] CO gas 3.7 (purity > 99.97%), Linde, Germany. Gas exposures were performed by backfilling of the vacuum chamber using leak valves. For the pressure measurements, which have an error of 20 %, we employed a Bayard-Alpert type ionization gauge. The different gauge sensitivities for N_2 (used for calibration) and CO were compensated by dividing the meter reading by a factor of 1.1.

desorption of molecules in direct contact with the surface; i.e., the sum of the peaks γ, δ, and ε constitutes the monolayer (ML). Accordingly, the sharp β peak (37 K) is associated with the second layer, and the non-saturating α peak (≥ 32 K) with the third and all further layers (multilayer adsorption or condensation). These assignments are supported by the relative peak intensities and also by UPS and Δφ results, as will be explained in more detail below.

Relative coverages were determined by numerical integration of thermal desorption spectra. In order to obtain *absolute* coverage values, the mass spectrometer signal was related to the absolute particle flux through the orifice using the effusion equation as described in Section 4.1.6. The error of the absolute coverage determined by this method equals that of the pressure measurement, 20%. The monolayer (ML) coverage is defined here as the maximum number of molecules in direct contact with the metal surface, with the binding energy, as determined by TDS, as the criterion for this 'direct' contact. According to this definition, the saturated CO ML contains $(7.1\pm1.5)\times10^{18}$ molecules per m^2, which is equivalent to 1.67±0.35 molecules in the 2.89 Å × 8.16 Å unit cell.

For all first-layer desorption maxima, the desorption activation energies, E_{des}, were estimated using the Redhead formula, Eq. 4.12, in which the first-order frequency factor ν_1 was approximated by $k_B T_{max}/h$. The respective E_{des} values are displayed in Fig. 8.1. E_{des} for the peaks α and β was obtained from a leading-edge analysis as described in Section 4.1.3. The value of 8.3 kJ/mol for α is in good agreement with the sublimation enthalpy of CO, 8.31 kJ/mol at 32 K [An67], and thus also a confirmation of a reliable sample temperature reading.

For a closer inspection of the CO sub-monolayer range, a set of TD spectra for initial coverages ranging from 0.12 ML to 1.54 ML, obtained by exposures between 0.15 L and 3.0 L, is displayed in Fig. 8.2. Notably, the desorption maxima within the sub-monolayer range, especially ε, shift substantially towards lower temperatures as the initial coverage increases. This shift suggests the operation of substrate-mediated long-range repulsive interactions, which indicate that CO modifies the electronic structure of the surrounding substrate. The much larger shift of the ε peak as compared to δ suggests that ε is associated with chemisorbed CO, which likely influences the surface electronic structure more effectively than the weakly bound, probably physisorbed δ-CO species. The coexistence of chemisorbed and physisorbed CO in the first layer is in agreement with a recent RAIRS study of CO adsorption on Au(110) at 300 K [Ju02]. In that work, a weakly chemisorbed CO species with a significantly reduced C-O stretching frequency relative to free CO was observed at CO pressures above 0.01 torr. At and above 100 torr, the signal of a further species with a vibration frequency close to the gas phase value was detected, which may correspond to our δ-CO species. It can easily be shown that a physisorbed CO species with the same desorption energy as δ-CO (as given in Table 1) may reach an equilibrium coverage of 0.07 (+0.05/-0.03) ML at 300 K and a CO pressure of 500 torr. This coverage is sufficient to be detected in a RAIRS experiment.

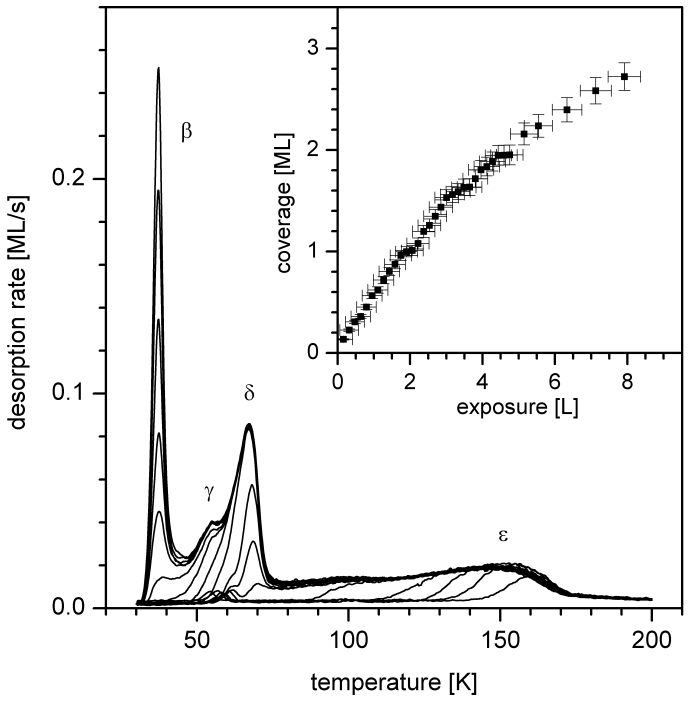

Fig. 8.2: CO TDS series for low and medium coverages, taken with a heating rate of 2.35 K/s. The spectra correspond to the following initial coverages (in ML): 0.12; 0.22; 0.33; 0.40; 0.49; 0.59; 0.63; 0.73; 0.87; 0.95; 1.00; 1.07; 1.20; 1.28; 1.34; 1.45; 1.54. Inset: Coverage (as determined by integration of the TD spectra in Fig. 8.2 and further spectra) vs. exposure.

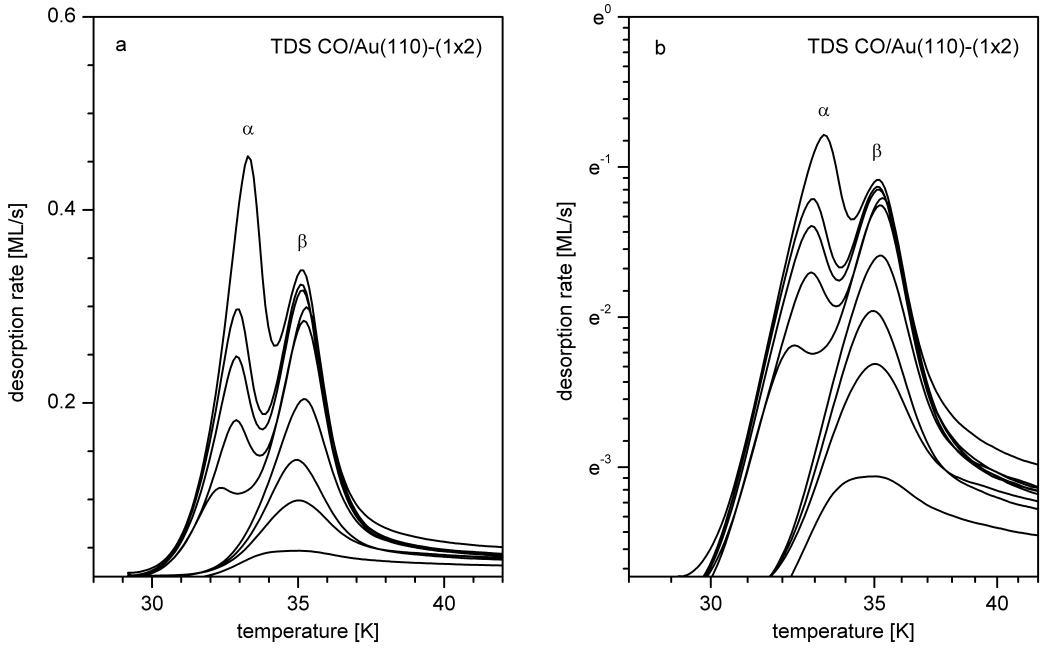

Fig. 8.3: Low-temperature range of a CO TDS series for high coverages. Heating rate 1.00 K/s. Initial coverages (in ML): 1.49; 1.67; 1.78; 2.00; 2.33; 2.44; 2.60; 2.70; 3.04. Note the logarithmic intensity and the reciprocal temperature scale in graph (b).

The γ-CO peak possibly arises from the relaxation of a densely packed phase which is formed as the ML is nearly complete ('decompression' peak). This assignment is supported by the fact that adsorption into the γ state is accompanied by a reduced sticking coefficient, as shown in Fig. 8.5. This peak will be further discussed in the context of the work function measurements (see Section 8.4).

The low-temperature parts of several high-coverage TD spectra are displayed in Fig. 8.3 for initial coverages between 1.36 ML and 3.04 ML. The high-temperature shift of both α and β and the lack of common leading edges suggest desorption orders between 0 and 1 with $n \to 0$ for α and $n \to 1$ for β. According to the order plot in Fig. 8.4, the desorption orders are $n_\alpha = 0.35 \pm 0.38$ and $n_\beta = 0.83 \pm 0.16$.

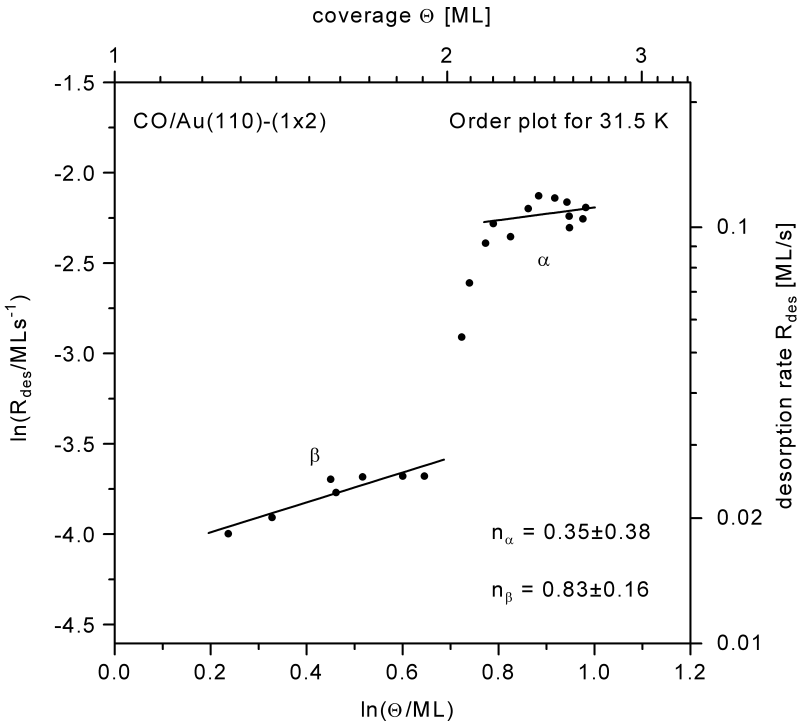

Fig. 8.4: TDS CO/Au(110)-(1×2). Order plot for T = 31.5 K.

	β-CO	δ-CO	ε-CO
E_{des} [kJ/mol]	9.5±0.6	18.5±1.3	38.4±2.8
ν_1 [s^{-1}]	$3.2\times10^{13\pm1}$	$3.0\times10^{14\pm1.3}$	$2.9\times10^{13\pm1.7}$

Table 8.1: CO/Au(110)-(1×2): Desorption energies and frequency factors for selected sub-monolayer desorption states, as evaluated from a heating rate variation analysis.

Desorption activation parameters were also evaluated by analysing the shift of the desorption maxima caused by a varying heating rate. This method was in detail explained in Section 4.1.3. For an initial CO coverage of 2.0 ML and heating rates between 0.25 K/s and 2.5 K/s, we obtained the values displayed in Table 8.1. Deviations of the true desorption order from the assumed, n = 1, would only affect ν and not E_{des}.

The frequency factor of ε agrees, within its margins of error, with the universal frequency factor, $k_B T_{max}/h = 3.1\times10^{12}$ s^{-1} (at T_{max} = 150 K). As shown elsewhere [Dr74], this value suggests a mobile adsorbate layer, in agreement with the results of the adsorbate entropy measurements discussed in Section 8.5. For immobile adsorption, transition state (TS) theory [Ey35, Gl41, Ey44] predicts a significantly higher ν_1 of 5.6×10^{15} s^{-1} for a TS with two translational degrees of freedom (DOF) and 4.1×10^{16} s^{-1} for a TS with one additional rotational DOF.

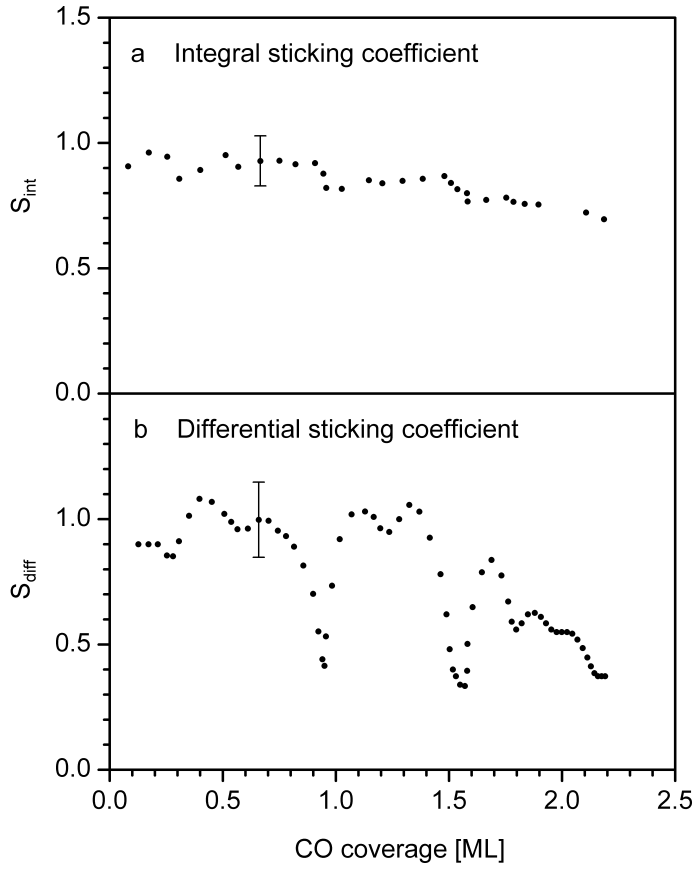

Fig. 8.5: Sticking coefficients for CO adsorption at 28 K. (a) Integral sticking coefficient $S_{int} = \Theta_{CO}/D_{CO}$ (with the CO dosage D_{CO}). (b) Differential sticking coefficient $S_{diff} = d\Theta_{CO}/dD_{CO}$. The curve was interpolated and smoothed after differentiation.

The CO sticking coefficient was determined by comparing the number of dosed molecules, as calculated by the collision flux equation, with the number of desorbed molecules, which was determined by TDS as described in Section 4.1.6. In the limit of zero coverage, we found a value of $S_0 = 0.9 \pm 0.1$ for adsorption at 28 K. The coverage dependence of the integral sticking coefficient, S_{int}, is displayed in Fig. 8.5a. More instructive is the differential sticking coefficient, $S_{diff}(\Theta_{CO})$, because it indicates the actual sticking probability for a particle impinging on a surface with the pre-coverage Θ_{CO}. In contrast, $S_{int}(\Theta_{CO})$ is the mean value over $S_{diff}(\Theta_{CO})$ for all coverages up to Θ_{CO}. $S_{diff}(\Theta_{CO})$, which is plotted in Fig. 8.5b, has minima in the range of the 'decompression' peak γ-CO and around 1.5 ML, a coverage that corresponds to a maximum in the Δφ curve (see Section 8.4).

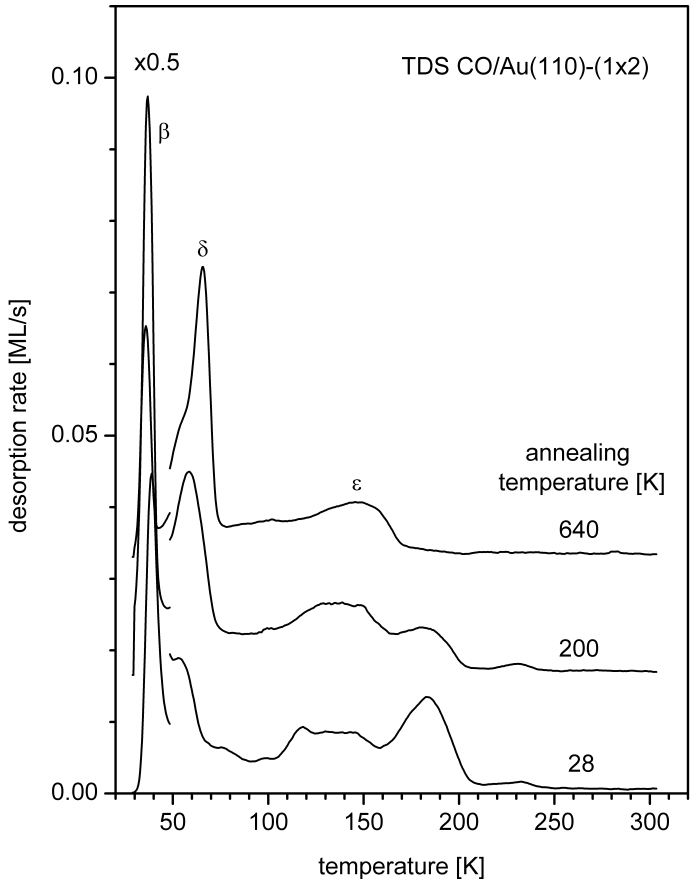

Fig. 8.6: TD spectra of CO on the ion-bombarded Au(110)-(1×2) surface, taken without prior annealing and after annealing at 200 K and 640 K. Ion bombardment at 28 K for 30 minutes with Ne^+ (750 eV, 1.0 μA/cm^2), CO dosage ≈ 4 L at a sample temperature of 28 K, heating rate 1.25 K/s.

CO DESORPTION FROM DEFECT SITES – Outka and Madix [Ou87a] studied the interaction of CO with Au(110)-(1×2) above 125 K and found no CO adsorption at all in the investigated temperature range. Therefore, one may suspect that our high-temperature desorption state ε monitors CO adsorption on defect sites rather than adsorption on the ordered surface. However, LEED provides no evidence for such a high defect concentration. In order to discriminate between adsorption on regular and on defect sites, we ion-bombarded the Au(110)-(1×2) surface with Ne^+ ions (750 eV) at 28 K and adsorbed CO directly after this treatment as well as after annealing at elevated temperatures. The resulting desorption traces are displayed in Fig. 8.6. The ion impact produces defect sites which lead to *additional* desorption states at higher temperatures around 184 K and 230 K, and not to an increased intensity of ε, as would be expected if ε was due to adsorption on defects. Annealing obviously reduces the defect concentration in general and leads to a decrease in the intensity of the respective desorption peaks. We annealed at temperatures between 50 K and 900 K and found changes in the TD spectra up to 500 K. At higher temperatures, the curves remained unaltered. Apparently, the defects induced by ion impact heal below 500 K. In conclusion, we attribute the desorption state ε to submonolayer CO adsorption on the well-defined Au(110)-(1×2) surface, in accordance with results of Dückers and Bonzel [Dü89], who estimated a maximum coverage of ≈0.3 ML CO on Au(110) at 117 K from photoemission experiments.

KRYPTON DESORPTION FROM CO/AU(110)-(1×2) – The conclusion that the broadening of the ε-CO peak reflects repulsive interaction between the CO molecules and is *not* caused by adsorption on defects sites is supported by another experiment, in which we used the noble gas krypton as a local probe for monitoring possible adsorption sites on clean and CO-precovered gold. Krypton desorbs from clean Au(110)-(1×2) completely below 75 K. A Kr TD spectrum with an initial coverage of 1.05 ML, curve (a) in Fig. 8.7, exhibits three maxima γ, δ, and ε, all of which belong to the first layer and a shoulder, β, around 43 K, that we associate with desorption from the second Kr layer. If we now populate the ε-CO state prior to the Kr adsorption, we can measure a complete Kr TD spectrum without simultaneous CO desorption, because the desorption ranges of ε-CO and Kr are well separated. Since CO is the more strongly bound species, it is likely that adsorption and desorption of Kr occurs on sites hitherto unoccupied by CO. The curves (b) and (c) in Fig. 8.7 show TD spectra of 3.2 L (1.05 ML) Kr taken after pre-adsorption of 0.3 and 0.6 ML CO. A prominent feature in curves (b) and (c) is the second-layer peak β-Kr, which grows since the first layer is already partially filled with CO. The three Kr monolayer peaks are not symmetrically damped by the CO pre-adsorption: γ-Kr and δ-Kr are more affected than ε-CO. We conclude that the desorption peaks ε-CO and (γ,δ)-Kr stem from the same adsorption sites. Returning to the question of whether or not defect sites are responsible for ε-CO, we can state that the ε-CO sites produce, in the case of Kr, one or two *sharp* desorption peaks, i.e., the broadening of ε is indeed connected to CO and not to ill-defined sites on our sample.

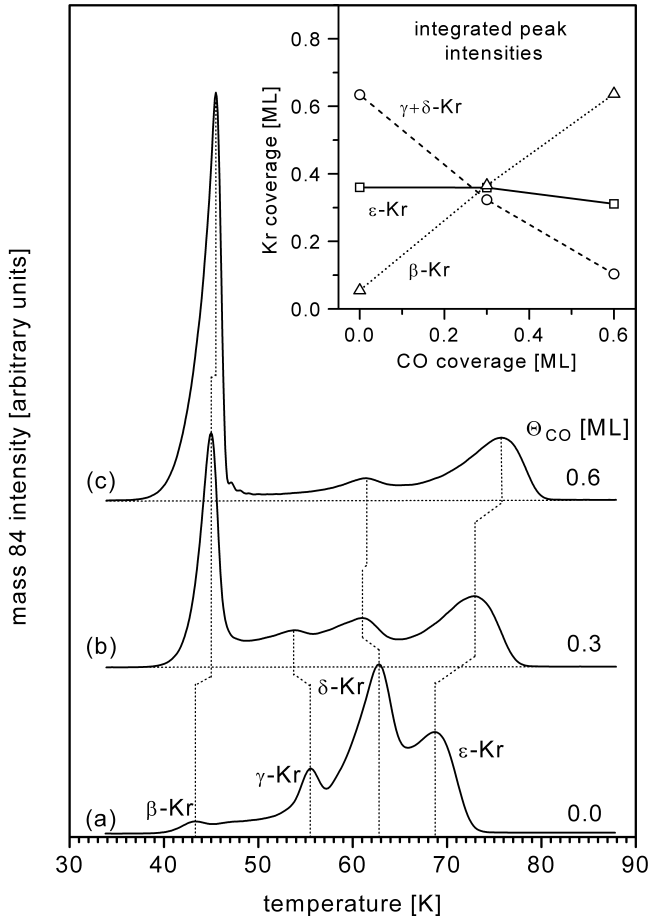

Fig. 8.7: Krypton (m/z = 84) thermal desorption spectra from (a) clean and (b,c) CO-precovered Au(110)-(1×2), heating rate 0.75 K/s. The Kr exposure[2] (always 3.2 L) corresponds to a coverage of 1.05 ML on the clean surface (curve a). The respective CO coverages were adjusted by adsorbing a CO excess at 30 K followed by heating to 120 K (curve b) and 75 K (curve c). Thereafter, the sample was again cooled to 30 K prior to the Kr adsorption. Inset: integrated peak intensities.

As a second important result, the most favourable sites for CO adsorption, giving rise to ε-CO, were found to be less favourable for Kr, since they lead to the low-temperature desorption states γ-Kr and δ-Kr. This observation likely reflects the fact that CO and Kr exhibit a different type of the adsorptive bonding, since one might otherwise expect the same sites to be equally favoured (especially if we consider the similar van-der-Waals radii of CO (1.99 Å) and Kr (1.97 Å) [Da67]). It is reasonable to assume that the Kr atom is attracted to the surface mainly by forces of the van-der-Waals type. The fact that ε-CO prefers different adsorption sites than Kr suggests that orbital-orbital interaction, i.e. chemisorption, largely contributes to the CO-surface bond. As a further result, the presence of ε-CO weakens the Kr-surface bond in the case of the competing desorption states

[2] Kr 4.0 gas, purity 99.99%, Messer Griesheim. The pressure meter reading was divided by a factor of 1.86 to account for the higher gauge sensitivity to Kr relative to N_2.

(γ+δ)-Kr, probably due to short-range repulsive interactions, whereas the ε-Kr peak, whose intensity is less affected by the presence of CO, shifts to higher temperatures and broadens. The difference in the desorption temperature, $\Delta T_{max} = 7.1$ K, corresponds to an increase in the binding energy of 1.9 kJ/mol or ≈11%, if we assume a constant frequency factor of $k_B T_{max}/h \approx 1.5\times10^{12}$ s^{-1}. The local modification of the surface electronic structure, caused by the ε-CO molecules, obviously stabilizes the ε-Kr state.

8.2. UV-photoemission measurements

TDS revealed the existence of two clearly separated groups of CO adsorption states with different desorption energies within the first layer, ε and (δ, γ). In agreement with this result, the CO UP spectra change strongly with coverage. Below 0.5 ML, i.e., in the range

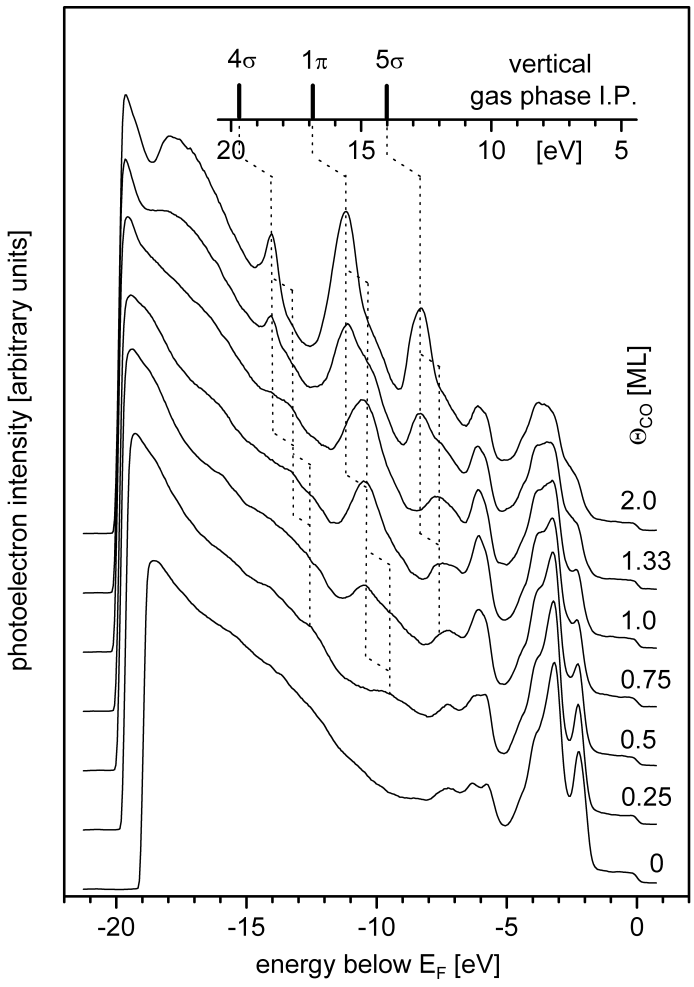

Fig. 8.8: UP spectra (hν = 24 eV) of CO/Au(110)-(1×2) for several CO coverages. Sample temperature 28 K, M polarization, normal emission. Gas phase values after [Tu70]. The energy scales (with reference to E_F and E_{vac}, respectively) were aligned by shifting the gas phase spectrum by $\varphi_0 + \Delta\varphi$ with $\varphi_0 = 5.37$ eV (Ref. [Hü96] in agreement with our measurements) and $\Delta\varphi = -0.95$ eV according to Section 8.4. Sample bias -10 V.

of ε-CO, the UP spectra of Fig. 8.8 and the difference spectra in Fig. 8.9 are dominated by a single broad peak around 9.4 eV. The other signals are weak; their positions are listed in Table 8.2 at the end of this chapter. Coverages above 0.5 ML, producing the δ-CO TD peak, lead to a further intense emission around 10.5 eV, which superimposes on the signal of the ε state. Additional clear signals at 7.8 and 13.3 eV appear as can be seen from the difference spectra in Fig. 8.9.

The emissions of condensed CO ($\Theta_{CO} > 1$ ML), whose energetic positions are listed in Table 8.2, can easily be related to the respective gas phase signals [Tu70]. Upon adsorption, all peaks shift to lower binding energies by ≈1.3 eV, which is mainly a final state effect arising from the additional extra-molecular relaxation of the final hole state in condensed CO.

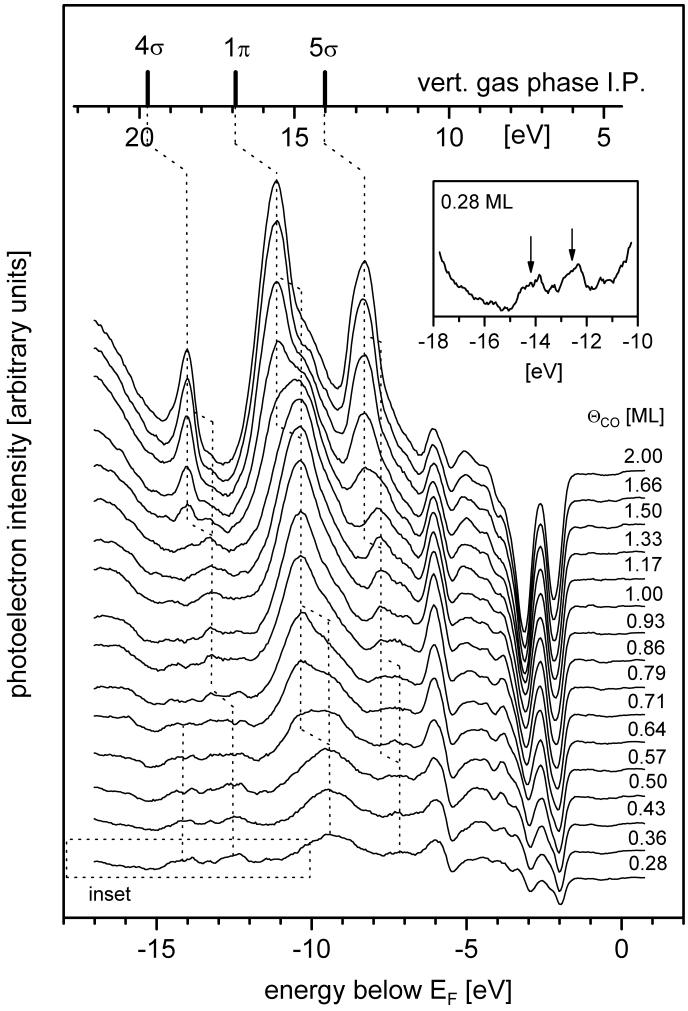

Fig. 8.9: UP difference spectra (hν = 24 eV) of CO/Au(110)-(1×2). The curves were obtained by subtraction of a spectrum of the clean surface. For the other parameters, see Section 4.2.2 and the caption of Fig. 8.8.

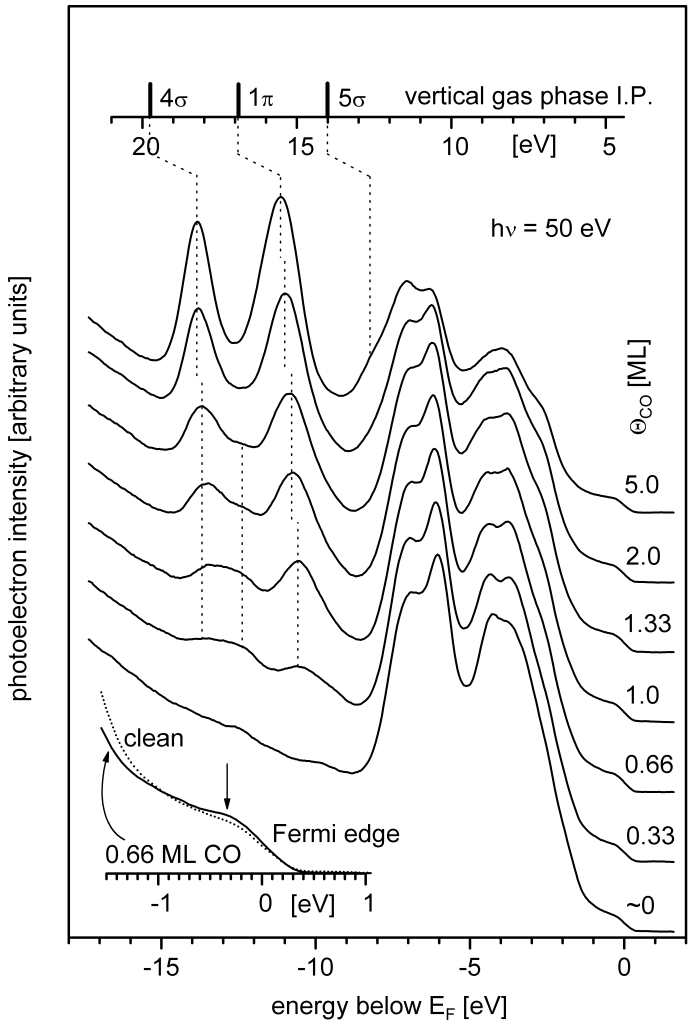

Fig. 8.10: UP spectra (hν = 50 eV) of CO/Au(110)-(1×2) for several CO coverages. Sample temperature 28 K, M polarization, normal emission. As in the preceding graphs, the gas phase spectrum was shifted by (φ + Δφ) with Δφ = 0.95 eV. A defect CO leak valve is responsible for a small CO pre-coverage (< 0.1 ML as determinded by Δφ measurements) in the spectrum of the 'clean' surface.

In the sub-monolayer range, the assignment of the emissions to the respective CO-MOs is less straight-forward. Between 0.5 ML and 1.0 ML, the low desorption energy of δ-CO, (18.5±1.3) kJ/mol, indicates a weakly bound, mainly physisorbed state. Therefore, the energetic spacing of the signals should be roughly the same as in the condensed phase, suggesting the following assignment of the peaks: 7.8 eV (5σ), 10.4 eV (1π), and 13.3 eV (4σ). If this assignment is correct, all signals undergo shifts towards lower binding energies of 0.4 eV (5σ), 0.8 eV (1π), and 0.7 eV (4σ) relative to the signals of the condensed phase. The occurrence of these shifts clearly indicates the growth of the second layer, while the differences show that the initial state (bonding) and final state (relaxation) contributions to these shifts are not equal for the particular levels. Unfortunately, due to the superposition of initial and final state effects it is difficult to derive information about the participation of the respective orbital in the surface chemical bond, unless both contribu-

tions are separated by means of a theoretical calculation. However, the major contribution is certainly the change of the (extra-molecular) relaxation energy due to the fact that the hole in photo-ionized CO is more effectively screened by the metal substrate (metallic screening) than by a matrix of other CO molecules in the condensed CO phase (dielectric screening).

Below 0.5 ML, the desorption energy of the ε-CO state, (38.4±2.8) kJ/mol, clearly indicates chemisorption, which generally causes major shifts of the CO emission states. The high intensity around 9.4 eV suggests an assignment to the (usually most intense) emission of the 1π level. The shift towards lower binding energies (relative to the emissions of the physisorbed δ-CO) points to anti-binding orbital interactions, if initial state effects prevail, or a more effective image charge screening, if final state effects dominate. We assign the weak signal around 7.2 eV to the 5σ orbital, although the respective emission may well be obscured by the intense Au 5d band signals between 2 eV and 8 eV below E_F. The 4σ signal is particularly difficult to trace because of its low cross section at the applied photon energy. There are still other weak, but clearly resolved emissions around 12.5 and 14.1 eV, and the former probably belongs to 4σ orbital excitation. The intensity of the 12.5 eV peak increases with the photon energy, as the 50 eV spectra in Fig. 8.10 and a comparison with literature data show. The shifts of the 12.5 eV signal in Fig. 8.9 indeed suggest the assignment to 4σ.

In order to obtain information about the orientation of the CO molecule on the surface, we performed polarization-resolved ARUPS measurements. The resulting spectra are presented in Fig. 8.11 and provide only minor evidence for CO molecules orientated parallel to the surface. The 9.4 eV (1π) peak of the (weakly) chemisorbed sub-monolayer ε-CO state is slightly less intense with X than with Z polarization, and the same applies for the 10.4 eV (1π) peak of the physisorbed δ-CO species. According to the dipole selection rules, this behaviour indicates a preferential orientation of the CO molecules parallel to the surface. The σ peaks, which should show the opposite changes, are too weak to further confirm this result[3]. At multilayer coverages, no polarization-dependent intensity changes were observed. All in all, the polarization-dependent effects remain small. A possible explanation is beam damage induced by the photon beam and the secondary electrons (see Section 8.7), which may disturb, in addition to other effects, a preferential orientation of the molecules.

[3] These experiments should be repeated with higher photon energies in order to obtain more intense σ peaks. Unfortunately, our access to polarized UV radiation ended with the shutdown of BESSY-I in December 1999, shortly after we had performed our first, the here presented, measurements on this system in November 1999.

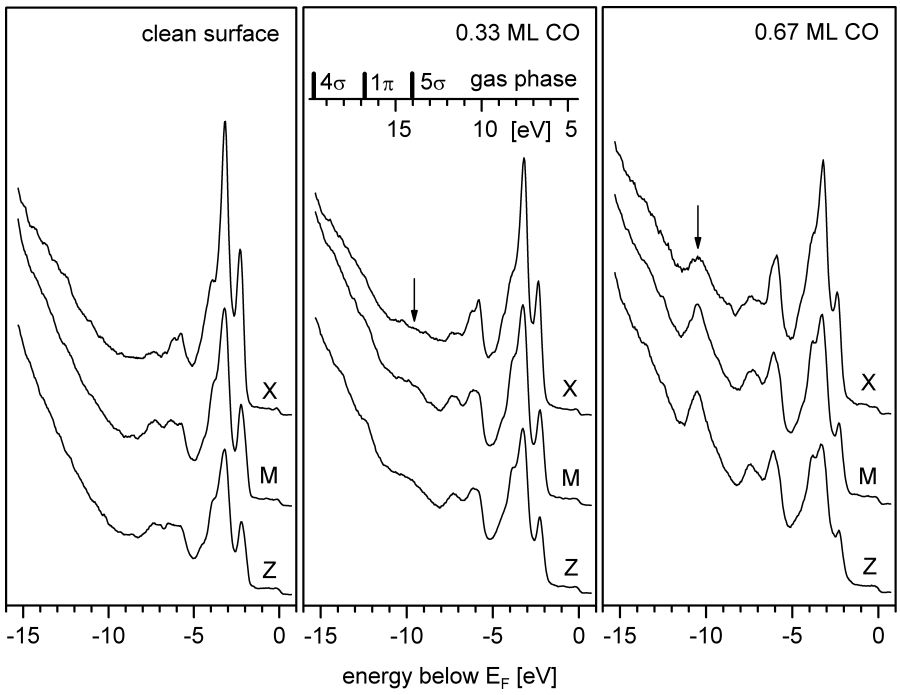

Fig. 8.11: Polarization-resolved UP spectra (hν = 24 eV) for CO/Au(110)-(1×2). The incidence angle of the linearly polarized UV light was varied in the $(00\bar{1})$ mirror plane (with the polarization vector parallel to that plane). The photoelectrons were detected in normal emission. See Section 4.2.2 for the geometric details of the experiment and for the meaning of X, M, and Z polarization. Sample bias -10 V. Significant changes in peak intensities are marked by arrows.

An orientation of the CO molecules parallel to the surface makes participation of the 5σ orbital in the CO-metal bond unlikely, i.e., binding interactions are restricted to the CO π orbitals. In this respect, bonding of CO to the gold surface differs from bonding to transition metals, for which the 5σ orbital plays a major role (Blyholder model [Bl64], see Section 2.2.2). In the case of gold, the 1π level can act as an electron donor and form a chemical bond with empty Au levels. However, this mechanism appears not effective since the Au d-levels are not only completely occupied but located ≈2 eV below E_F, and the next empty metal levels are Au 6p with a relatively high energy. It should be taken into account, however, that truncation of the metal bulk at the (110)-surface may introduce unoccupied d-states at the surface. Neglecting this possibility, back donation from Au 5d levels into the CO 2π* orbital should generally be more effective since relativistic effects enhance the energy of the former and thereby reduce the energetic difference between the interacting orbitals, which increases the interaction energy. This 2π*-5d hybridization should influence the intensities in the Au 5d band, but the variations are certainly too small to be observed in the presence of other effects such as the suppression of the d-band intensity by photoelectron scattering. Because the CO 5σ orbital cannot contribute, the CO-surface bond resembles that of ethylene, C_2H_4, and can be described by the Dewar-Chatt-Duncanson model [De51, Ch53]. This correspondence is probably the

reason for the striking similarities between CO and C_2H_4 adsorption on gold, which is considered in more detail in Chapter 9.

Comparison of our CO/Au UP spectra with literature data, as displayed in Table 8.2, is hindered by the fact that the experimental conditions, especially CO coverage and temperature, were often ill-defined in previous work. Additionally, the photon energy, which strongly influences the relative peak intensities, was higher in the previous studies and ranged from 40.8 eV to 150 eV.

Nevertheless, the occurrence of three peaks in our sub-monolayer spectra contrasts sharply with the findings on many transition metals [Hü96], for which the strong metal-CO orbital interactions cause peak shifts which regularly lead to a complete overlap of the 5σ and 1π emissions. Our spectra rather resemble, apart from the exact peak positions, those for CO/Ag(110) [Kr84], which are also dominated by three CO-induced peaks. The peak separations in the case of CO/Ag were close to those found in the gas phase spectrum, and the peaks were assigned to the 4σ, 1π, and 5σ levels. Relative to the gas phase, the peaks showed a rigid shift of about 0.7 eV towards lower binding energies, which was explained by the image potential screening due to the substrate. Accordingly, CO/Ag(110) was classified as a physisorbed system [Kr84]. In a further CO/Ag(110) UPS study [Sa94], performed with a photon energy of 125 eV, the authors confirmed the appearance of three peaks, but other results led to the conclusion that the CO/Ag system has to be regarded as chemisorbed, which made the former assignment of the peaks at 14.8, 12.1 and 9.5 eV to the 4σ, 1π and 5σ levels questionable. One feature that suggests chemisorption was an enhanced intensity right below E_F, which was attributed to 2π*(CO)-sp(Ag) hybrid states. We note here that, in our UPS experiments with a photon energy of 24 eV, CO adsorption led to a *reduced* intensity in the region of the Au 6sp band. However, the spectra excited with 50 eV radiation as displayed in Fig. 8.10 (inset) show an increased intensity close to E_F, which could in fact be the result of a weak 2π*(CO)←sp(Au) back-bonding interaction.

In the above-mentioned work [Sa94], UP spectra of CO on Au(110) were also reported. The authors claim to have produced a saturated CO ML on a gold sample cooled with liquid nitrogen. They note that the CO coverage remained rather low, but attribute this to the fact that the Au(110) surface is reconstructed. Comparison with our TD spectra in Fig. 8.2 reveals that cooling with l-N_2 is not sufficient to achieve ML coverage under UHV conditions and that Sandell et al. hardly reached 0.5 ML. The UP spectrum ($h\nu$ = 150 eV) corresponding to this coverage exhibited two peaks at 9.8 and 12.6 eV below E_F and a weak feature at 13.7 eV. These signals were assigned, in analogy to CO/Cu(100) and by comparison with C1s autoionization spectra for CO/Au(110), to 5σ/1π, 4σ, and a satellite, respectively. In the respective coverage range (Θ_{CO} < 0.5 ML), our spectra ($h\nu$ = 24 eV) show emissions at 7.3 eV (5σ), 9.4 eV (1π), 12.5 eV (4σ), and a weak feature around 13.8-14.5 eV. For assigning the emissions to the indicated orbitals it proved advantageous to have a complete coverage series ranging from sub-monolayer to multilayer coverages at our disposal. The observed monotonous peak shifts indeed

strongly support our assignment given in Table 8.2. Interestingly, an enhanced intensity in the region of the Au 5d band at 6 eV is observed, which is highest around monolayer coverage and also occurs in the UP spectra of C_2H_4/Au(110)-(1×2), as shown in Chapter 9. A similar effect can be seen in the CO/Ag(110) UP spectra reported by Sandell et al. [Sa94], but no interpretation was given in that work.

Norton et al. [No78] studied CO adsorption on a polycrystalline gold sample. In a He-II excited spectrum ($h\nu = 40.8$ eV) of ≈ 0.2 ML CO adsorbed at 77 K they found two peaks and one shoulder. The CO-gold interaction was characterized as chemisorptive, and the emissions were deconvoluted into four components at 9.6, 10.3, 12.3, and 13.3 eV, results that do not differ much from our findings. One major difference, however, is the higher intensity of the 12.3 eV signal compared to our spectra, an effect which may be due to the different photon energies applied.

8.3. LEED

No ordered CO overlayers could be observed with LEED in the whole temperature (≥ 28 K) and coverage range ($0 < \Theta_{CO} \leq 15$ ML). This result is in agreement with all previous reports on CO adsorption on Au [Mc76a, Sa94, Ru96] and with the findings for CO on Ag(111) [Mc76]. It differs, however, completely from the results for CO on Cu, for which ordered overlayers were found e.g. on Cu(100) [Ch71] and Cu(111) [Ch73]. McElhiney and Pritchard [Mc76a] and, later, Ruggiero and Hollins [Ru94] studied CO/Au(100) and CO/Au(332), respectively and argued that the low CO coverages obtained in their experiments, which remained indeed below ≈ 0.5 ML according to our estimation, are responsible for this lack of long-range order. Nonetheless, the argument certainly does not apply to our observations. As a possible explanation for our results, the long-range order of the weakly bound CO molecules may be disturbed by the electron beam. The problem of beam damage is considered in detail in Section 8.7.

Carbon monoxide adsorption does not lift the 1×2 reconstruction of the Au(110) surface, whereas the reconstructed Pt(110)-(1×2) surface is easily transformed into the 1×1 structure when CO is adsorbed at room temperature [Mo69, Bo73, Co76, He76]. The reconstruction of Ir(110)-(1×2) seems also to be stable against CO adsorption [Ch73a]. (The three surfaces, the only (110) metal surfaces which undergo a 1×2 reconstruction, were briefly discussed in Chapter 2.1.)

The lack of ordered CO phases prevents us from establishing a structural model of the adsorbate layer. Instead, some information can be derived from a comparison of the packing densities of adsorbed and solid CO. The latter has a molecule density of $\rho_{3D} = 0.022$ Å^{-3} [An67], which is equivalent to $\rho_{2D} = \rho_{3D}^{2/3} = 0.079$ Å^{-2} in two dimensions. This value agrees well with our measured absolute coverage of (0.071±0.015) Å^{-2}. This means, the CO monolayer consists of a densely packed phase.

The specific suppression of Kr thermal desorption peaks by CO pre-adsorption as described in Section 8.1 may allow the identification of CO adsorption sites, if the Kr desorption peaks can be assigned to the respective sites. The necessary investigations are presently performed in our laboratory [Sc03].

8.4. Work function measurements

The CO induced work function change, $\Delta\varphi$, upon adsorption at 28 K is displayed in Fig. 8.12 as a function of (a) exposure and (b) coverage. At low coverages, in the range of the ε-CO desorption state, φ decreases strongly and almost linearly with Θ_{CO}. Depolarization effects seem to play a minor role; the repulsive CO-CO interactions seen in TDS (Fig. 8.2) seem to keep the CO molecules apart. In this linear region, the Helmholtz equation (Eq. 4.48) can be applied to determine the initial dipole moment, μ_0, of the individual adsorption complex, if the absolute CO coverage, σ_{CO}, is known. With the value for σ_{CO} given in Section 8.1, we obtained $|\mu_0| = (0.93\pm0.20)$ D.

Above 0.5 ML, in the region of the δ-CO peak, the distance between the molecules is reduced due to the higher CO coverages, resulting in a strong mutual depolarization of the adsorbate-induced dipoles. This is indicated by a plateau in the $\Delta\varphi$ vs. Θ_{CO} curve (Fig. 8.12b) between ≈ 0.5 and ≈ 0.8 ML.

As the CO coverage approaches 1.0 ML, a further work function decrease by ≈ 0.1 eV coincides with the occupation of the γ-CO desorption state. In Section 8.1, we interpreted this peak as being caused by relaxation of a compressed CO monolayer. $\Delta\varphi$ suggests that the compression could be accompanied by a (partial) erection of the flat-lying CO molecules. As a result, the molecular dipole moment of CO, μ_{CO}, acquires a component perpendicular to the surface, which influences the surface potential.

A minimum in the $\Delta\varphi$ curve is obtained at a coverage of 1.11 ML. The small maximum around 1.50 ML also falls in the second-layer range and coincides with a minimum in the differential sticking coefficient as displayed in Fig. 8.5b. The structure in this region reflects the arrangement of the CO dipoles in the second layer and suggests that the molecules are no longer parallel to the surface in this layer, since otherwise no effect of μ_{CO} on the work function would be observed. This interpretation is consistent with our polarization-resolved ARUPS measurements and with the fact that these features in the $\Delta\varphi(\Theta_{CO})$ curve are not present if CO is replaced by the non-dipolar C_2H_4, which shows apart from that a very similar behaviour in TDS and $\Delta\varphi$ (see Chapter 9). Above 2 ML, the work function is approximately constant at $\Delta\varphi = -0.95$ eV or, in terms of absolute values, $\varphi = 4.42$ eV.

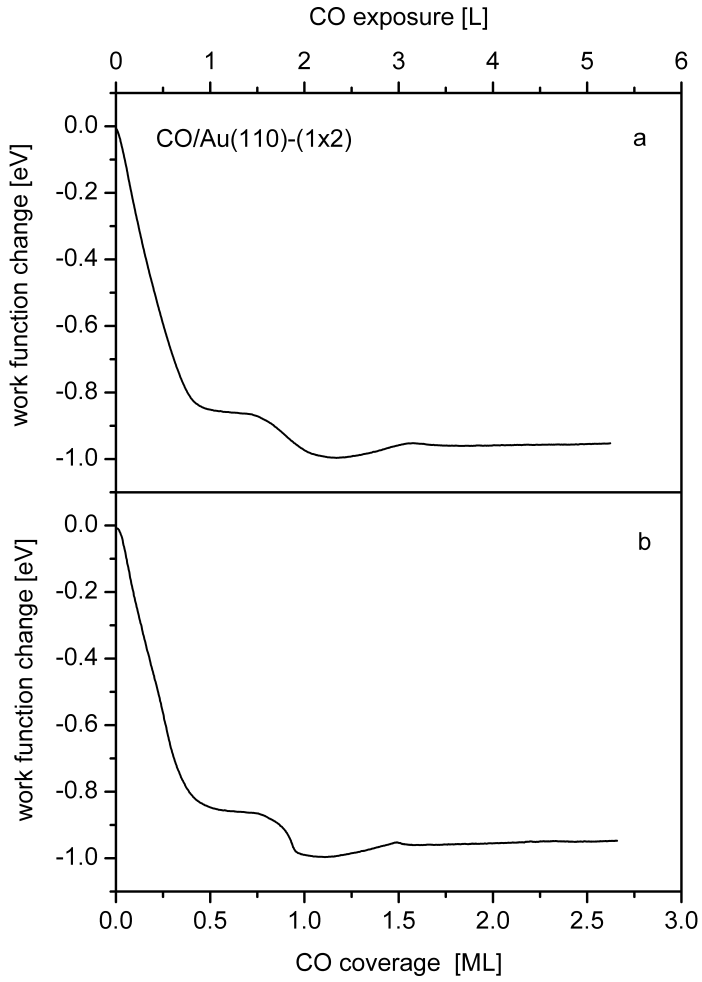

Fig. 8.12. CO induced work function change vs. (a) exposure and (b) coverage upon adsorption at 28 K and $p_{CO} = 2\times10^{-8}$ mbar. Conversion of exposures into coverages according to Fig. 8.2, inset.

The fact that the work function *decreases* upon CO adsorption may also serve as an indication that the molecule is only weakly chemisorbed or physisorbed on Au(110)-(1×2). CO adsorption on transition metals often leads to a work function *increase* of 1 eV or more. The negative work function change of CO/Au(110)-(1×2) agrees well with the previous studies of CO adsorption on gold and is also in line with the negative changes caused by CO on Cu and Ag. CO adsorbed on Au(332) at 92 K led to a work function decrease of -0.47 eV at an unknown CO coverage maintained by a CO background pressure of 1×10^{-6} mbar. The CO coverage was probably far from saturation [Ru96]. CO adsorption on Au(100), studied at 81.5 K and 4.4×10^{-4} Pa CO, caused a $\Delta\varphi$ of -0.85 eV; the coverage here was also uncertain [Mc76a]. On Ag(110), CO adsorption decreased the work function by -0.8 eV at ≈ 1 ML CO coverage [Kr84]. Typical of CO adsorption on Cu is a pronounced work function minimum in the sub-monolayer range, which may correspond to the plateau region in our $\Delta\varphi$ curve. As an example, the $\Delta\varphi$ curve of

CO/Cu(100) shows a minimum (-0.2 eV) around 0.35 ML CO [Tr72]; many other $\Delta\varphi_{min}$ values down to -0.47 eV for CO/Cu(111) are reviewed in Ref. [Pa75].

8.5. Isosteric heat and adsorbate entropy

The $\Delta\varphi(\Theta_{CO})$ curve in Fig. 8.12b shows that the adsorbate-induced work function change can be employed as a monitor of the equilibrium CO coverage for $\Theta_{CO} < 0.5$ ML. The function $\Theta_{CO}(p_{CO},T)$ obtained in this way can be used to evaluate thermodynamic adsorption quantities such as the isosteric heat, Q_{st}, or the partial molar entropy, ΔS_{ads}. For this purpose, we measured several adsorption isobars, $\Delta\varphi(T)_p$, which are displayed in Fig. 8.13. From these curves, we extracted triples $(p_{CO},T,\Delta\varphi)$, converted $\Delta\varphi$ into Θ_{CO}, and rearranged the triples (p_{CO},T,Θ_{CO}) to adsorption isotherms, $\Theta_{CO}(p_{CO})_T$, as shown in Fig. 8.14.

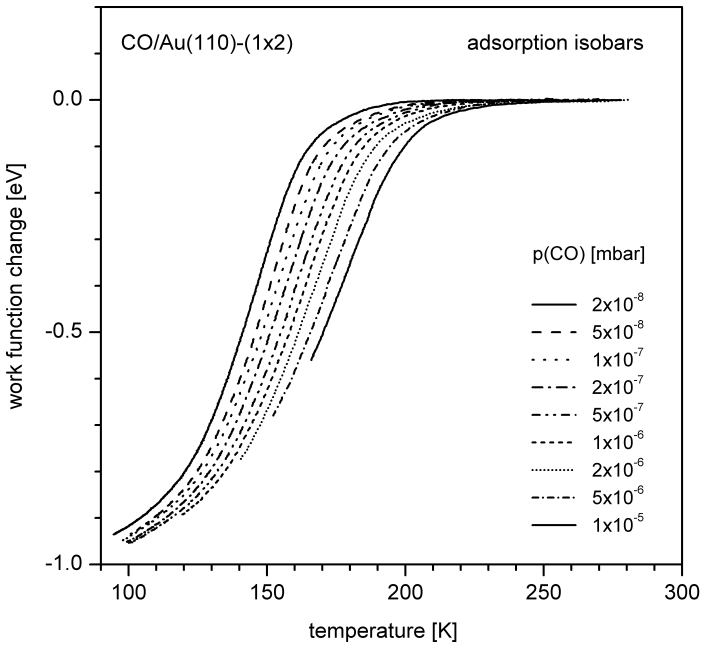

Fig. 8.13: Adsorption isobars for CO/Au(110)-(1×2).

The adsorption-desorption equilibrium can be described by the Clausius-Clapeyron equation, Eq. 3.1, according to which plots of $\ln \tilde{p}_{CO}$ vs. 1/T for fixed Θ_{CO}, as presented in Fig. 8.15, are straight lines with gradients that depend on the isosteric heat at this coverage, $Q_{st}(\Theta_{CO})$. The coverage dependence of $Q_{st}(\Theta_{CO})$, extracted from a number of isosteric plots, is displayed in Fig. 8.16.

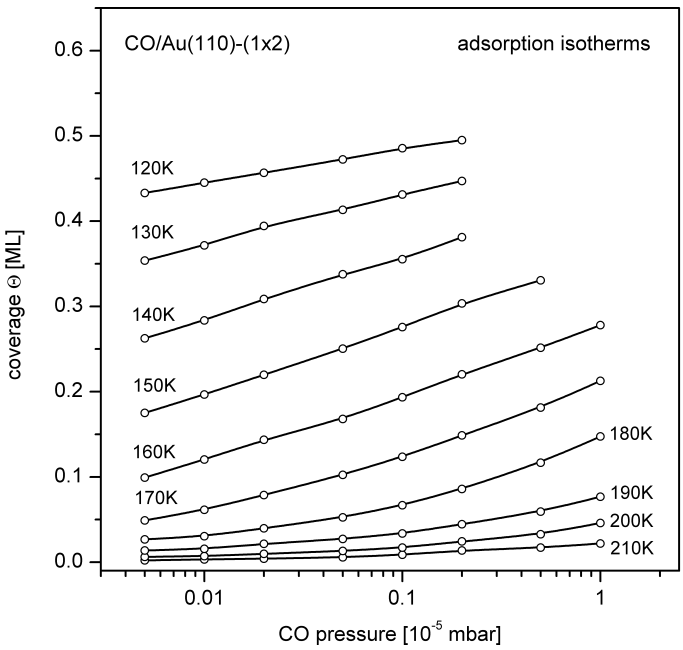

Fig. 8.14: Adsorption isotherms for CO/Au(110)-(1×2). See text for the details.

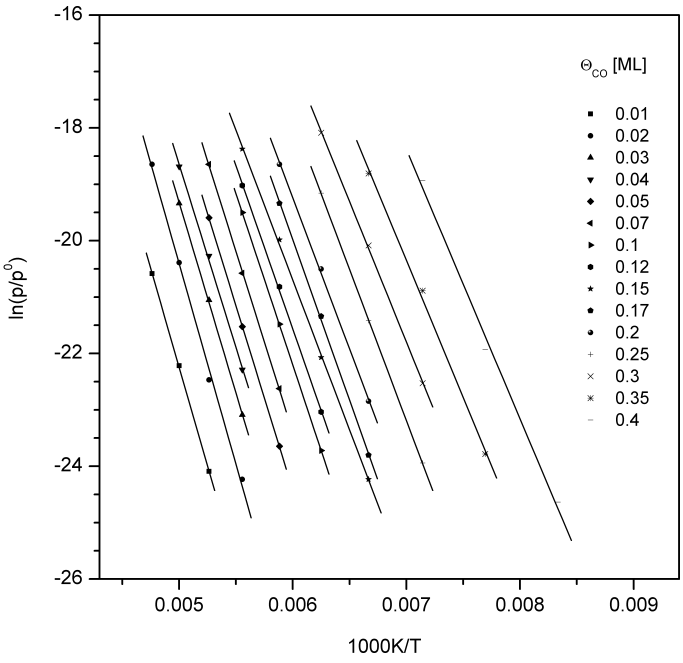

Fig. 8.15: Isosteric plots for CO/Au(110)-(1×2).

Extrapolation to $\Theta_{CO} \rightarrow 0$ yields an initial isosteric heat of 59±2 kJ/mol, which is in good agreement with the value of 58±3 kJ/mol found by McElhiney and Pritchard [Mc76a] for CO adsorption on Au(100). Slightly lower is the value for CO/Au(332), 55±3 kJ/mol, reported by Ruggiero and Hollins [Ru96]. Thus, the initial heats for CO adsorption on gold are generally closer to the values found for CO on copper (e.g. 70 kJ/mol on Cu(100) [Tr72], 61±2 kJ/mol on Cu(311) [Pa75]) than for CO on silver (e.g. 27±1.5 kJ/mol on Ag(111) [Mc76]).

According to equipartition considerations as described in Chapter 3, the adsorbate binding energy, $|E_0|$, of a diatomic molecule depends on the isosteric heat as follows:

$$|E_0| = \begin{cases} Q_{st} & \text{for mobile adsorption} \\ Q_{st} - \frac{3}{2}RT & \text{for immobile adsorption} \end{cases} . \qquad \text{(Eq. 8.1)}$$

A discussion of the adsorbate entropy below suggests a mobile adsorbate. Thus, $|E_0|$ is equal to Q_{st} and, if the adsorption is non-activated, also equal to the desorption activation energy E_{des}.

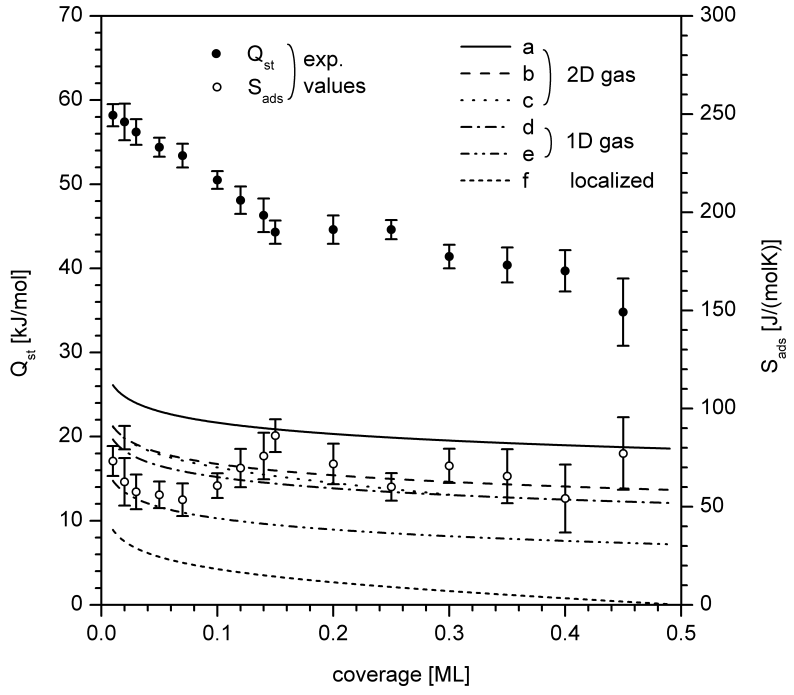

Fig. 8.16: Isosteric heat of adsorption (full circles, left axis) and partial molar entropy of the adsorbate at 160 K (open circles, right axis). Calculated entropies of a two-dimensional CO gas at 160 K: (a) $S_{tr,2D}^{perfect} + S_{rot}$; (b) $S_{tr,2D}^{perfect}$; (c) $S_{tr,2D}^{real}$. Calculated entropies of a one-dimensional perfect gas: (d) $S_{tr,1D}^{perfect} + S_{rot}$; (e) $S_{tr,1D}^{perfect}$. (f) Calculated entropy for localized adsorption, $S_{2D,loc}$. (The error bars increase for $\Theta_{CO} \rightarrow 0.5$ ML since the work function varies only little with Θ_{CO} in this range (see Fig. 8.12b). For the same reason, coverages above 0.5 ML are not accessible.)

A comparison of $|E_0|$ with E_{des} as determined by TDS analysis can answer the question of whether the adsorption is activated or not. For this comparison, both energies must be referenced to the same coverage. The value of $E_{des} = (38.4 \pm 2.8)$ kJ/mol given in Table 8.1 applies to the ε-CO desorption maximum with a residual CO coverage of 0.15 ML. The corresponding value of $|E_0|$ is (42.0 ± 1.4) kJ/mol. Since activated adsorption would require $E_{des} > |E_0|$, CO adsorption on gold is clearly non-activated.

As mentioned above, the catalytic CO oxidation on supported gold clusters already sets in below room temperature. The present models for the reaction mechanism favour the adsorption of CO on the gold particles. It is therefore reasonable to ask for the CO coverage around $p^0 = 1$ atm and 300 K. Extrapolation of the isosteres in Fig. 8.15 reveals that at 320 K and $p_{CO} = p^0$ a CO coverage of 0.4 ML is reached – a very favourable value for a (catalytic) surface reaction.

Further information about the configuration of the CO adlayer can be deduced from the partial molar entropy of the adsorbate, S_{ads}, which is, according to Chapter 3, given by:

$$S_{ads} = \Delta S_{ads} + S_g = -\frac{Q_{st}}{T} + \left\{ S_g^0 - R \ln \frac{p_{CO}}{p^0} \right\} \qquad \text{(Eq. 8.2)}$$

(with the standard gas phase entropy $S_g^0 = S_g(p^0)$ at the standard pressure $p^0 = 1$ atm, and the partial molar adsorption entropy ΔS_{ads}). Fig. 8.16 displays S_{ads} at a temperature of 160 K.

Within the framework of statistical thermodynamics, S_{ads} depends on the degrees of freedom available for the adsorbed particles. In the following discussion, we treat several adsorbate states between two limits: (a) the completely mobile case of a two-dimensional (2D) gas phase with translational and rotational freedom, and (b) the completely localized case with only configurational entropy. We find that these limits cover all experimental entropy values.

The translational part of the partial molar entropy of a 2D perfect gas is [Cl70]:

$$S_{tr,2D}^{perfect} = R \left\{ \ln \left[\frac{2\pi m_{CO} k_B T}{h^2} \frac{b_{CO}}{\Theta_{CO}} \right] + 1 \right\} \qquad \text{(Eq. 8.3)}$$

with the mass of the CO molecule, m_{CO}, and the area occupied per CO molecule at saturation, $b_{CO} = 1.4 \times 10^{-19}$ m^2. The value for b_{CO} is derived from the absolute coverage given in Section 8.1. The other symbols have their usual meaning. In Fig. 8.16, curve (b), Eq. 8.3 is plotted for T = 160 K.

Consideration of the area excluded by the finite size of the molecules leads to the following equation for the translational part of the partial molar entropy of the 2D gas:

$$S_{tr,2D}^{real} = R\left\{\ln\left[\frac{2\pi m_{CO} k_B T}{h^2}\frac{b\,(1-\Theta_{CO})}{\Theta_{CO}}\right] - \frac{1}{1-\Theta_{CO}} + 2\right\}. \qquad \text{(Eq. 8.4)}$$

A plot of Eq. 8.4 is shown in Fig. 8.16, curve (c).

The CO molecule may also rotate around an axis normal to the surface. This degree of freedom leads to an additional entropy contribution of:

$$S_{rot} = \tfrac{1}{2} R\left\{\ln\frac{T}{\Theta_{rot,CO}} + 1\right\} \qquad \text{(Eq. 8.5)}$$

with the rotational temperature of CO, $\Theta_{rot,CO} = 2.77$ K [Mc73]. At 160 K, S_{rot} is 21.02 J(mol K)$^{-1}$. Curve (a) represents $S_{tr,2D}^{perfect} + S_{rot}$, i.e., the entropy of a perfect 2D gas with two translational and one rotational degree of freedom.

The particular structure of the reconstructed Au(110) surface may also allow a one-dimensional (1D) translation of the molecules along the trenches. Curve (d) shows the case of 1D translation and rotation; curve (e) considers only 1D translation.

In the limit of localized adsorption, the adsorbate has only configurational entropy:

$$S_{2D,loc} = R\,\ln\frac{1-\Theta_{CO}}{\Theta_{CO}}, \qquad \text{(Eq. 8.6)}$$

which is plotted in Fig. 8.16, curve (f).

For coverages above 0.1 ML, the measured entropy S_{ads} is, within the experimental error, in agreement with both theoretical curves (b,c) for the 2D translational entropy. The curves (b,c) differ by less than the experimental error. Adding one rotational degree of freedom makes the theoretical entropy too large (curve (a)). Obviously, the 2D gas with (partially) frozen molecular rotation is an appropriate model for describing the adsorbed CO phase at this temperature and in this coverage range. The hinderance of the rotational motion may result from adsorption at the bottom of the deep trenches in $[\bar{1}10]$ direction, which are characteristic for the 1×2-reconstructed Au(110) surface.

At very low coverages, $\Theta_{CO} < 0.08$ ML, the experimental entropy nearly coincides with curve (e), which represents 1D translation. We may conclude that the high binding energy

in this coverage range limits the adsorbate mobility. As Q_{st} decreases with growing Θ_{CO}, the molecules increasingly acquire translational freedom, and the entropy rises, between 0.10 and 0.15 ML, rapidly to values typical for a 2D gas. Above 0.1 ML, S_{ad} is also well described by curve (d), which represents 1D translational and rotational freedom.

With S_{ads} known we can also determine the entropy of the desorption transition state, $S^0_{\neq}$, which is given by:

$$S^0_{\neq} = S^0_{ads} + \Delta S^0_{\neq} \approx S_{ads} + R \ln \frac{h\nu_1}{k_B T} \qquad \text{(Eq. 8.7)}$$

In Eq. 8.7, we considered that $S_{ads} \approx S^0_{ads}$, since the entropy of the adsorbate (as a quasi-condensed phase) depends only weakly on gas pressure. Furthermore, we applied the well-known relation between activation entropy, $\Delta S^0_{\neq}$, and the desorption frequency factor, ν_1 (see Eq. 3.10). Eq. 8.7 yields $S^0_{\neq} = (105\pm42)$ J(mol K)$^{-1}$ at 150 K and 0.15 ML (i.e., at the desorption maximum of ε-CO). This value agrees well with the entropy of a 2D gas with one excited rotation at this temperature, 91 J/(mol K), and it is much smaller than the gas phase value, which is S^0_{gas} = 176 J(mol K)$^{-1}$ at 150 K [Da67].

8.6. NEXAFS measurements

A series of normal-incidence CO NEXAFS spectra, taken at 28 K, is displayed in Fig. 8.17. The spectra exhibit a π* resonance at 534.7 eV due to excitation into the unoccupied 2π* orbital and, visible only at higher coverages, a σ* resonance at 550.9 eV.

According to Ref. [St92], the width and, to a lesser extent, the position of the π* resonance are affected by the strength of the 2π*←metal backbond. Since the molecule remains neutral in the excitation process, relaxation effects arising from extra-molecular screening effects are small, and any shift of the π* resonance is mainly due to initial state effects, i.e., it reflects the binding interactions of the 2π* orbital. Thus, significant backbonding should lead to different widths and positions of the π* peak for sub-monolayer and multilayer coverages. The spectra in Fig. 8.17 reveal that the π* positions are constant within ±0.1 eV, the widths within ±0.15 eV, in other words, both are constant within the noise level. We conclude that the 2π*-metal orbital interactions are weak, a result that is consistent with our TDS and UPS findings.

No significant differential changes in the peak intensities occurred upon variation of the beam incidence angle parallel to the $(00\bar{1})$ plane (with the vector potential parallel to that plane). However, the identification of small effects would have required low-noise measurements with prolonged data acquisition. Those measurements led to considerable beam damage as explained in Section 8.7, probably also caused by the secondary electrons. Possibly, the beam and the emitted secondary electrons also disturb a preferential

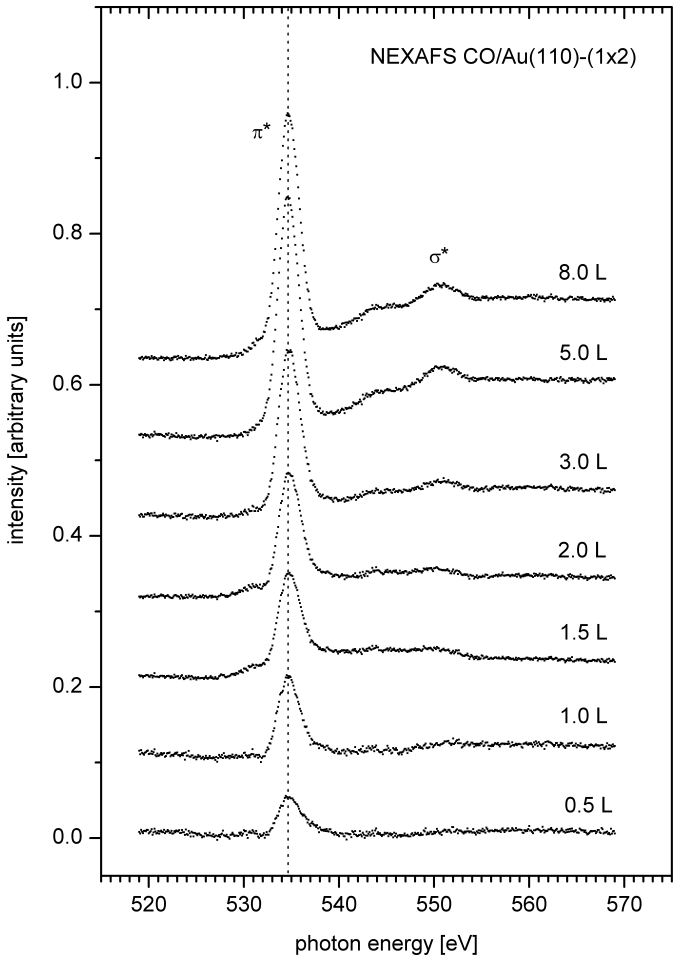

Fig. 8.17. Normal incidence NEXAFS spectra of CO/Au(110)-(1×2) at 28 K. The polarization vector was parallel to the [$\bar{1}$10] direction, i.e., to the trenches of the reconstructed (110) surface. The spectra are corrected for differences in the photon flux, but not normalized to the step between the onset of the π* resonance and the continuum. See text for the details and Section 4.5 for the experimental details.

orientation of the CO molecules on the surface. This process requires far less energy than the irradiation- (or electron-) induced dissociation of the molecule, which we consider in the following section.

8.7. Beam damage

We have obtained evidence that CO/Au adsorbates undergo reactions under the influence of electron or photon irradiation, although no systematic study of these effects, as in the case of CO/Ni(110) [Ve79] or O_2/Au(110) (Chapter 5), was carried out. LEED investigations revealed that electron bombardment of CO at 28 K for several minutes with beam intensities typical of a routine LEED study led to a reduction of the substrate spot intensities and to an increased background signal. This behaviour is similar to that of O_2/Au,

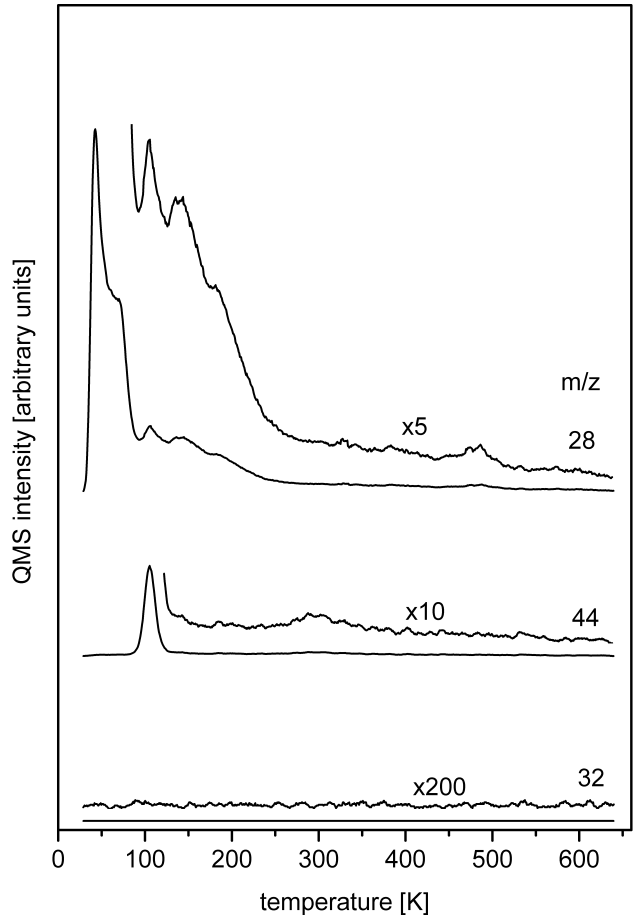

Fig. 8.18: TDS of an electron-bombarded CO layer (≈ 3 ML) on Au(110)-(1×2) with simultaneous detection of m/z = 28, 32, and 44. Heating rate 2.35 K/s. See text for the details.

but no complete extinction of the substrate spots took place. The original LEED pattern could not be restored by heating to 250 K, a temperature which is sufficient to completely remove unperturbed CO adlayers, suggesting that electron-induced activation of CO leads to the formation of strongly adsorbed, and probably fragmented, species. Only heating to ≈ 650 K gradually restored the LEED pattern.

In a further type of experiment, similar to those described in Chapter 5, we therefore bombarded CO multilayers with electrons emitted from a 'flood gun' and examined the resulting adsorbate layers with TDS. We applied an electron beam with a primary energy of 500 eV which produced an incident current density of 4.7 $\mu A/cm^2$ at the sample. Fig. 8.18 shows desorption traces of CO, CO_2, and O_2 taken after bombardment of 10 L (≈ 3 ML) CO at 28 K for 3 minutes under the above-mentioned conditions. Comparison of the mass 28 curve with the CO TD spectra in Figs. 8.1 and 8.2 reveals that the bombardment induces CO desorption at temperatures up to ≈ 270 K, in contrast to ≈ 170 K for the non-irradiated layer. This broadening towards higher temperatures could be due to the formation of defect sites under the influence of the electron impact. The TD spectrum,

however, differs significantly from that obtained after ion bombardment as shown in Fig. 8.6, which suggests that other factors, e.g. CO dissociation, come into play. The CO_2 signal around 105 K indicates that CO partially disproportionates to the thermodynamically more stable CO_2 and to carbon. Further signals appear on the CO curve around 480 K and on the CO_2 curve around 300 K, both of which must stem from the recombinative desorption of C and O atoms. No oxygen desorption is observed over the whole temperature range. One reason is that initially formed chemisorbed oxygen has already reacted with remaining CO below the O_2 desorption temperature of > 500 K. This reaction also provides an alternative explanation for the occurrence of the CO_2 signal around 105 K.

8.8. Conclusions

Carbon monoxide is weakly chemisorbed ($\Theta_{CO} < 0.5$ ML) and physisorbed ($0.5 \leq \Theta_{CO} \leq 1.0$ ML) on Au(110)-(1×2). For the chemisorbed CO, the isosteric heat of adsorption varies between 59 kJ/mol ($\Theta_{CO} \rightarrow 0$) and 35 kJ/mol ($\Theta_{CO} = 0.45$ ML). TDS reveals the existence of several adsorption states with typical desorption activation energies of 38.4 kJ/mol (0.15 ML), 18.5 kJ/mol (0.75 ML), and 9.5 kJ/mol (second layer). The extraordinary low-temperature shift of the TDS peak attributed to chemisorbed CO indicates substantial repulsive interactions between the CO molecules in the chemisorbed phase. This long-range repulsion is a further indication of chemisorption, since it proves that CO influences the electronic structure of the surface over extended distances. In UPS, we observed significantly different signals for chemisorbed and physisorbed CO. Polarization-resolved UPS provides evidence that the CO molecules are parallel to the surface. CO adsorption causes a negative work function change which corresponds to an initial dipole moment of the CO-Au complex of 0.93 D. Our NEXAFS data support the assumption of an only weakly chemisorbed system. Measurements of the adsorbate entropy and comparison with theoretical values shows that the state of the chemisorbed phase at 160 K can be described by a two-dimensional gas of CO molecules without rotational freedom. The fact that CO remains normally undissociated on the gold surface under the condition of our experiment allowed us to study beam damage and to show that electron bombardment of CO adlayers leads to dissociation of the molecules.

Substrate	T [K]	hν [eV]	Θ [ML]	Peak positions [eV] and assignment						Bonding state	Ref.	Remarks
Cu(poly)	20	40.8	≈0.5 (?)	8.7 (5σ)			11.6 (1π)		14.5 (4σ)	physisorbed	[No78]	prob. Θ >> 1 ML (condensed)
	30	40.8	≈0.3 (?)	8.5 (5σ/1π)			11.8 (4σ)	13.5 (sat)		chemisorbed	[No78]	probably Θ ≈ 1 ML
Cu(100)	>77	90	(2×2)-CO	8.6 (5σ/1π)			11.5 (4σ)	13.5 (sat)		chemisorbed	[Sa94]	
Ag(110)	50±3	40.8	≤1	9.1 (5σ)			11.9 (1π)		14.8 (4σ)	physisorbed	[Kr84]	molecules parallel to surface
	≈50	125	≈1	9.5 (5σ/1π)			12.1 (4σ)	14.8 (sat)		chemisorbed	[Sa94]	
Au(poly)	77	40.8	≈0.2	9.8			12.3	13.3			[No78]	no resolved peaks in CO TDS
Au(110)	117	132.3	≈0.3	10.0 (1π)			12.5 (4σ)	13.8 (sat)		chemisorbed	[Dü89]	
	>77	150	<0.5	9.8 (5σ/1π)			12.6 (4σ)	13.5 (sat)		chemisorbed	[Sa94]	
	28	24	0.25	7.3 w	9.4	-	12.5 w	13.8-14.5 w		chemisorbed	this work	w = weak {} = overlaps with peaks of physisorbed CO
			0.5	7.7 w	9.4	10.3	12.5 w	13.8-14.5 w	13.3 (4σ)	chemisorbed		
			1.0	7.8 (5σ)	{9.3}	10.4 (1π)	{12.5 w}	{13.8-14.5 w}	13.3 (4σ)	physisorbed		
			≥2.0	8.2 (5σ)	-	11.2 (1π)	-	-	14.0 (4σ)	condensed		
Gas phase I.P.*				14.01 (5σ)		16.91 (1π)			19.72 (4σ)		[Tu70]	vertical gas phase I.P.
I.P.-(φ_0+Δφ)				9.59 (5σ)		12.49 (1π)			15.30 (4σ)			φ_0 = 5.37 eV, Δφ = -0.95 eV

Table 8.2: UPS peak positions for CO/Au(110)-(1×2) and comparison with selected literature UPS data for CO adsorption on coinage-metal surfaces.